A comprehensive study on single and competitive adsorption-desorption of copper and cadmium using eco-friendly magnetite (Fe$_3$O$_4$) nanoparticles

Somayeh Bakhtiari*,†, **Meysam Shahrashoub***, and **Ali Keyhanpour****

*Department of Civil Engineering, Sirjan University of Technology, Sirjan, Iran
**Research & Development, Sirjan Jahan Steel Complex, Sirjan, Iran

Abstract–The present study investigated the capability of magnetite nanoparticles (MNP) synthesized from the direct reduction iron sludge and green tea extract for the single and competitive adsorption of copper (Cu^{2+}) and cadmium (Cd^{2+}). Moreover, we assessed the desorption of Cu^{2+} and Cd^{2+} in a ten-day cycle (both single and competitive systems) to evaluate their release amount from the adsorbent's surface. The adsorption process was described using three well-known adsorption isotherms: Langmuir, Freundlich, and Dubinin-Radushkevich. The Freundlich isotherm was employed to describe the desorption process. The maximum adsorption capacity of Cu^{2+} and Cd^{2+} by MNP according to the Langmuir curve was 21.24 and 19.36 mg/g, respectively. A significant difference was observed in the adsorbed value of heavy metals in the competitive mode and MNP selectively preferred Cu^{2+} against Cd^{2+}. Results of energy-dispersive X-ray (EDX) and elemental mapping analyses corroborated the Cu^{2+} and Cd^{2+} adsorption in both single and competitive systems. The findings of Fourier-transform infrared spectroscopy (FTIR) analysis revealed the role of functional groups in Cu^{2+} and Cd^{2+} adsorption. The results of the desorption evaluation demonstrated the higher tendency of MNP to retain Cu^{2+} than Cd^{2+}. We developed economical and environmentally friendly magnetite nanoparticles, promising in individual and competitive adsorption of Cu^{2+} from aqueous solutions while resisting to release it. Moreover, the adsorbent's performance in singular removal of Cd^{2+} was noticeable.

Keywords: Adsorption, Desorption, Competitive Adsorption, Heavy Metal Ions, Magnetite Nanoparticles, Water Pollution

INTRODUCTION

Environmental pollution, especially water contamination, is a continual concern. Among various pollutants, heavy metals arising from human activities, agricultural activities, diverse industries, domestic sewage, and other sources are a serious threat to the entire ecosystem, particularly the health of humans and other living species. Some of the influential industries include mining, paper production, leather fabrication, battery making, nuclear activities, fossil fuel combustion, and pigmentation [1-3].

Copper and cadmium are two important heavy metals that are predominantly utilized in the production industry [4] and should be considered due to their high toxicity, non-degradability, and the possibility of accumulation in the food chain [5,6]. Therefore, to prevent the entry of these pollutants into the environment and to diminish the subsequent adverse effects, the reuse and recycling of wastewater is inevitable [7,8]. The single presence of heavy metals in natural circumstances is a rare phenomenon and various kinds of metal ions often coexist simultaneously in wastewater of industries such as electroplating. Their interaction with each other and other substances in the environment, influences their transport and fate. The frequent presence of Cu^{2+} and Cd^{2+} in urban industrial wastewater makes it crucial to investigate their multicomponent adsorption characteristics in both single and binary metal solutions [4,9].

In the case of reusing treated water for human consumption or discharge to the environment without following unfavorable impacts, there is need for wastewater treatment using suitable method. Wastewater treatment progress requires advanced methods and equipment [7,8]. Numerous techniques, namely coagulation [10], membrane filtration [11,12], adsorption [13,14], electrochemical approaches [15,16], distillation [17], electrodialysis [18,19], ion exchange [20,21], photocatalytic methods [22], and biological treatments [23,24], have been proposed to remove heavy metals from aqueous solutions. Each of these approaches has some advantages and disadvantages. Adsorption is effective for the removal of various pollutants, including heavy metals because of low operating costs, insignificant sediment production, optimal economic efficiency, no secondary pollutants, high controllability, and excellent removal capability [2,3,6,25].

Adsorption is a mass transformation method in which contaminants enter the active sites of adsorbents through physical or chemical processes [26,27]. It is highly necessary to choose the right adsorbent for the adsorption process. Various adsorbents, such as silica gel, activated carbon, biochar, polymer compounds, agricultural waste, biomaterials, industrial waste, nanomaterials, metal oxides, graphene, and some other materials have been evaluated and utilized as adsorbents [1,2,13,28].

In recent years, nanosorbents have received much attention due to their unique properties, including possessing functional groups,

†To whom correspondence should be addressed.
E-mail: Bakhtiari@sirjantech.ac.ir

active adsorption sites, photocatalytic features, antibacterial effects, as well as electrical, optical, and magnetic properties [29]. In addition, the highly selective nature of nanosorbents makes them effective for the removal of certain contaminating ions in a competitive condition with other ions [30]. The efficiency of adsorption might be affected by some factors, such as the type of heavy metal, the presence of other heavy metals, and adsorbent properties [31]. Metal oxide nanosorbents have been widely used and recommended for the treatment of heavy metals in wastewater [1]. Synthesizing these nanosorbents using mining and industrial metal wastes with a green method highlights their importance [32].

So far, numerous investigations have been conducted on the synthesis of magnetite nanoparticles (MNP) and their application in heavy metals removal [33-35]. Almost all previous studies have focused on the utilization of commercial iron salts or mineral wastes, e.g., iron ore tailings as their iron source. The synthesis of MNP via the co-precipitation method requires a stoichiometric mixture of ferric and ferrous iron in an alkaline medium or only ferric iron source in the presence of a reducing agent for producing ferrous iron. The majority of studies have used commercial iron salt in the presence of a chemical or natural reducing agent to synthesize MNP [36-38]. In the case of applying mineral and industrial waste as the source of iron, a chemical reducing agent has been used for the synthesis [35,39]. No study except our previous research [40] has ever synthesized magnetite nanoparticles using steel-making industrial waste and a natural reducing agent simultaneously.

Despite the high efficiency and selectivity of MNP in removing heavy metals from aqueous solution [41], no research has yet evaluated the use of green synthesized magnetite nanoparticles using industrial wastes for both single and competitive adsorption and desorption of heavy metals. Therefore, the present study aimed to investigate the capability and efficiency of green synthesized MNP for the single and binary adsorption and desorption of Cu^{2+} and Cd^{2+} to simulate their behavior in natural environments.

MATERIALS AND METHODS

1. Materials

In this study, direct reduction iron (DRI) sludge, a by-product of the steelmaking process, was used as the primary source of iron. The DRI sludge was obtained from Sirjan Jahan Steel Complex, Iran. All the utilized chemicals were of high purity and were purchased from Merck (Germany), including 37% hydrochloric acid (HCl), copper sulfate ($CuSO_4 \cdot 5H_2O$), cadmium chloride ($CdCl_2 \cdot H_2O$), and calcium chloride ($CaCl_2 \cdot 2H_2O$). In addition, Tala green tea (Iran) was applied as the natural reducing agent.

2. Methods

2-1. Synthesis of MNP

MNP was synthesized as described in our previous study [40]. In summary, to synthesize magnetite nanoparticles, the iron content of the DRI sludge was extracted using hydrochloric acid and was selectively precipitated as iron hydroxide ($Fe(OH)_3$) and used as a ferric iron source. To obtain a 2 : 1 ratio of ferric to ferrous iron, a portion of Fe^{3+} was reduced to Fe^{2+} using green tea extract. Moreover, MNP was synthesized by co-precipitation technique in an alkaline medium using NaOH. According to our previous study,

instrumental studies, such as XRF, XRD, FESEM, HRTEM, SAED, EDX, elemental mapping, DLS, zeta potential, FTIR, BET, VSM, and TGA/DSC revealed the proper synthesis of MNP [40].

2-2. Adsorption and Desorption Experiments

In this study, heavy metal contaminated effluent was artificially fabricated in the laboratory. Since distilled water is not able to simulate natural wastewater conditions due to the lack of electrolyte ions, Calcium chloride ($CaCl_2$) salt was used to solve this problem. To study the adsorption of Cu^{2+} and Cd^{2+}, $CuSO_4$ and $CdCl_2$ salts were dissolved in 0.01 M $CaCl_2$ medium, respectively. First, a stock solution containing 1,000 mg/L of each heavy metal was prepared. The desired concentrations of Cu^{2+} and Cd^{2+} in the range of 5-400 mg/L were prepared using the dilution method. The release of adsorbed ions after the completion of the adsorption process can be considered secondary pollution. To evaluate this issue, desorption tests were performed immediately at the end of adsorption tests.

2-2-1. Single and Competitive Adsorption Experiments

The impact of initial concentration on the single adsorption of Cu^{2+} and Cd^{2+} was examined separately. For this purpose, 10 ml of heavy metal solutions with the primary concentrations of 10, 50, 100, 150, 200, 300, and 400 mg/L of Cu^{2+} and Cd^{2+} was equilibrated with 0.1 g of adsorbent for 24 h in three replicates. After achieving pseudo-equilibrium, the supernatant was separated from the solid phase. The equilibrium concentration of heavy metal ions in the solution was determined using the AAnalyst800 (Perkin Elmer, USA) atomic absorption spectrometer (AAS). In the following, the experimental data from single adsorption were fitted with the experimental models of Langmuir, Freundlich, and Dubinin-Radushkevich.

To investigate the competitive adsorption of Cu^{2+} and Cd^{2+}, a binary system of the mentioned elements with the initial concentrations of 5, 10, 25, 50, 75, 100, 150, 200, 300, and 400 mg/L of both elements was prepared. Similar to the single adsorption, 0.1 g of adsorbent was suspended with 10 ml of each solution in three replications for 24 h. At the end of the pseudo-equilibrium, the solid phase was separated from the solutions and the remaining concentration of both heavy metals in the solution was measured. For each of the concentrations of Cu^{2+} and Cd^{2+} in both single and competitive modes, a control sample without adsorbent was considered. The amount of adsorbed ions was quantified based on the difference between the concentration of the control sample and equilibrium concentration in the solution per unit mass of adsorbent (mg/g).

2-2-2. Single and Competitive Desorption Experiments

To assess the release rate of adsorbed ions on the surface of the adsorbent and examine the occurrence of hysteresis phenomenon, desorption tests were immediately performed after the adsorption process in a 10-day cycle. In the single mode, samples with the initial concentrations of 100 and 300 mg/L were evaluated in three replications, while samples with the primary concentrations of 50 and 150 mg/L were tested in binary mode. To simulate the natural water conditions, a 0.01 M calcium chloride solution was used during the cycle. After combining the adsorbents with 10 ml of calcium chloride, the suspensions were placed in an incubator shaker (FTSH-501 L, SCI Fintech, South Korea) for 24 h at 150 rpm and room temperature. The solution was separated from the adsorbent and was replaced with 10 ml of fresh 0.01 M calcium chloride in

each day of the cycle to evaluate the amount of the released ion. The concentration of desorbed heavy metals in each cycle was measured using an AAS. Finally, the Freundlich model was fitted to the data obtained from the desorption procedure and the hysteresis indices were calculated.

2-3. Adsorption and Desorption Modeling and Data Analysis

The adsorption modeling of experimental data was performed by Langmuir, Freundlich, and Dubinin-Radushkevich mathematical equations. The Langmuir isotherm assumes that monolayer adsorption occurs on a uniform surface with a limited number of adsorption sites [42]. Freundlich isotherm is applied to multilayer adsorption processes on the heterogeneous surface and active sites with different energy [43]. The Dubinin-Radushkevich isotherm does not presume constant adsorption potentials or homogeneous surfaces. Therefore, this model is more generic than Langmuir. It is utilized to evaluate the mean energy of sorption, and determine the nature of the adsorption, whether it is physical or chemical [44]. The general form of the Langmuir [45], Freundlich [46], and Dubinin-Radushkevich [47] empirical equations are presented in Eqs. (1)-(3), respectively.

$$q_e = \frac{q_{max}K_L C_e}{1 + K_L C_e} \tag{1}$$

$$q_e = K_{F, ads} C_e^{n_{ads}} \tag{2}$$

$$q_e = q_{m, DR} e^{-K_{DR}\varepsilon_{DR}^2} \tag{3}$$

In the expressed equations, the parameters are defined as follows:

q_e: adsorption amount at equilibrium (mg/g), q_{max}: maximum adsorption capacity of Langmuir isotherm (mg/g), K_L: Langmuir isotherm constant (L/mg), C_e: equilibrium concentration of adsorbate ions in aqueous solutions (mg/L), $K_{F, ads}$ and n_{ads}: Freundlich constants for adsorption data, $q_{m,DR}$: maximum adsorption capacity of Dubinin-Radushkevich isotherm (mg/g), K_{DR}: Dubinin-Radushkevich isotherm constant (mol²/kJ²), ε_{DR}: Polanyi potential Dubinin-Radushkevich isotherm model (kJ/mol) which calculated from the following equation:

$$\varepsilon_{DR} = RT\ln\left(1 + \frac{1}{C_e}\right) \tag{4}$$

where R is the universal gas constant (8.314 J/mol·K), T is the absolute temperature (298.15 K) of adsorption process equilibrium, and C_e is equilibrium concentration of adsorbate ions in aqueous solutions (mol/L). In many previous studies, the equilibrium concentration of the Dubinin-Radushkevich model has been expressed in mg/L. In this case, the accuracy of the model calculations could be affected by the dimensional problem in the Polanyi potential equation. Zhou et al. [48] proposed a correction for this issue that included the equilibrium concentration (C_e) of Dubinin-Radushkevich in mol/L.

The adsorption free energy (kJ/mol) can be calculated from:

$$E = \frac{1}{\sqrt{2K_{DR}}} \tag{5}$$

The amount of adsorption free energy (E) determines the nature of adsorption (chemical or physical). If the value of E is lower than 8 kJ/mol, the adsorption process is of physical type, while if it is in the range of 8-16 kJ/mol, the adsorption is considered a chemical process [49].

In addition to the adsorption data, the results of single desorption of Cu^{2+} and Cd^{2+} were also fitted by the Freundlich model according to Eq. (6).

$$q_e = K_{F, des} C_e^{n_{des}} \tag{6}$$

where q_e: desorption amount at equilibrium (mg/g), and $K_{F, des}$ and n_{des}: Freundlich constants for desorption data.

2-4. Hysteresis Index

The adsorption and desorption coefficients of the Freundlich model are not independent, because the starting point of the desorption isotherm is a point of the adsorption isotherm. However, the value of K_{des} (Freundlich desorption coefficient) is usually different from K_{ads} (Freundlich adsorption coefficient). The n_{des}/n_{ads} exponential ratio indicates the presence or absence of hysteresis. Theoretically, in the absence of hysteresis, $n_{des}/n_{ads}=1$ and $K_{des}=K_{ads}$. Positive hysteresis is denoted by $n_{des}/n_{ads}<1$ and $K_{des}>K_{ads}$, and negative hysteresis indicates $n_{des}/n_{ads}>1$ and $K_{des}<K_{ads}$ [50]. Gao and Jiang [51] introduced Eqs. (7)-(9) to determine the hysteresis phenomenon and also expressed the positive and negative hysteresis as mentioned below.

$$H = \left(\frac{n_{des}}{n_{ads}}\right) \times 100 \tag{7}$$

$$\omega = \left(\frac{n_{ads}}{n_{des}} - 1\right) \times 100 \tag{8}$$

$$\lambda = \left(\frac{n_{ads}+1}{n_{des}+1} - 1\right) \times 100 \tag{9}$$

In the first state, when H=100, $\omega=0$, and $\lambda=0$, there is no hysteresis. In the second state, if H≠100, $\omega\neq0$, and $\lambda\neq0$, hysteresis exists. In this condition, if H>100, $\omega<0$, and $\lambda<0$, the hysteresis is negative and if H<100, $\omega>0$, and $\lambda>0$, the hysteresis is positive.

2-5. Characterization of the Spent Adsorbent

After the completion of single and competitive adsorption analyses of Cu^{2+} and Cd^{2+}, to investigate the adsorption process and articulate its mechanisms FTIR (Thermo, AVATAR, USA), elemental mapping, and EDX (SAMX detector, France) analyzes were conducted on the adsorbent.

RESULTS AND DISCUSSION

The adsorption of Cu^{2+} and Cd^{2+} was evaluated using MNP synthesized in our previous study [40]. The properties of MNP include an average particle size of 8 nm based on HRTEM analysis, a specific surface area of 68.84 m²/g, and magnetic field strength of 52.9 emu/g. Single adsorption experimental data were examined using Langmuir, Freundlich, and Dubinin-Radushkevich isotherms. Adsorption isotherms can reflect the reactions between adsorbent and adsorbate and express the possible adsorption mechanisms [52]. The form of isotherms is the first empirical tool for detecting the nature of adsorption [53].

1. Single Adsorption Studies

Fig. 1 shows the fitting of the data of Cu^{2+} and Cd^{2+} adsorption by Langmuir, Freundlich, and Dubinin-Radushkevich models. As
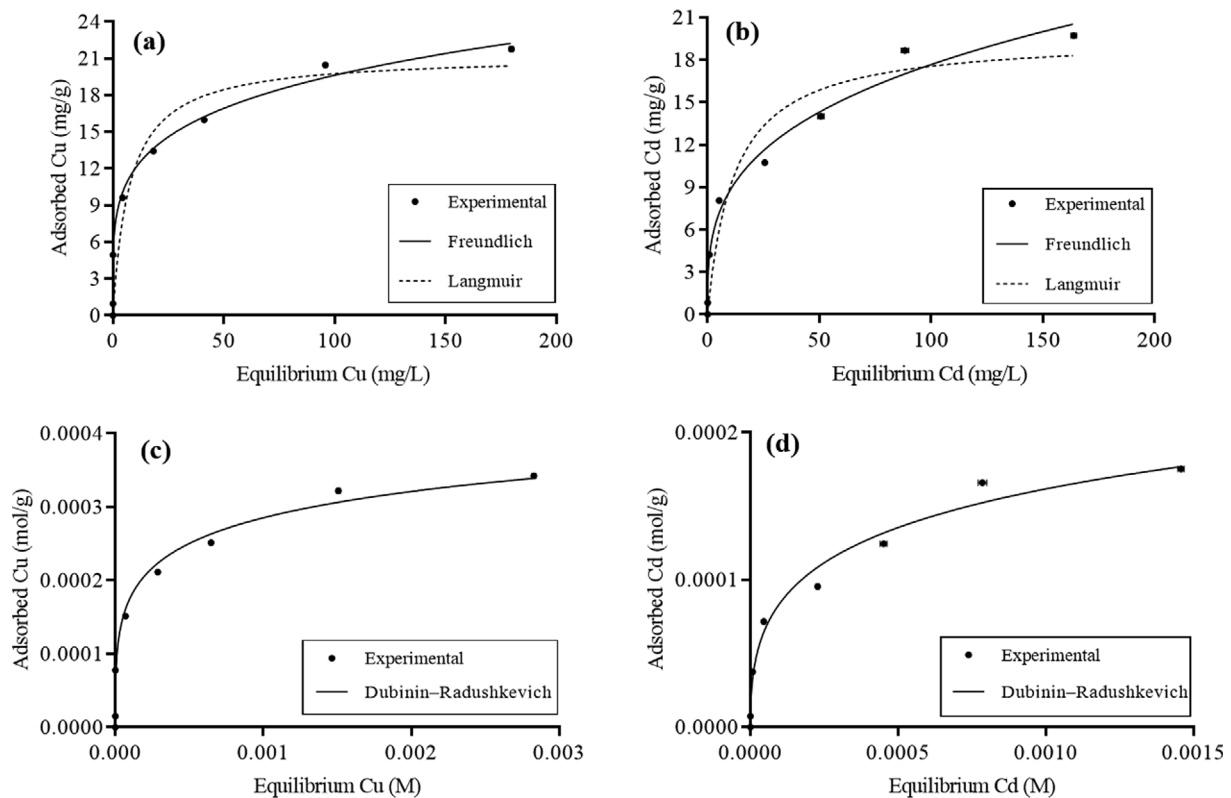
Fig. 1. (a) Fitting of Langmuir and Freundlich models to Cu^{2+} adsorption data, (b) Fitting of Langmuir and Freundlich models to Cd^{2+} adsorption data, (c) Fitting of Dubinin-Radushkevich model to Cu^{2+} adsorption data, (d) Fitting of Dubinin-Radushkevich model to Cd^{2+} adsorption data.

seen in Figs. 1(a) and 1(b), the plot of adsorbed ions (q_e) vs equilibrium concentration (C_e) for the Freundlich isotherm gives much better fit at all concentration ranges of Cu^{2+} and Cd^{2+}. According to the classification of Giles et al. [54], Langmuir adsorption diagrams are classified as L type, which implies a high affinity and interaction between adsorbate and adsorbent, especially in lower concentrations. The increase of Cu^{2+} initial concentration resulted in its adsorption rate. The graphs were almost linear at higher

concentrations, in which the adsorbent has reached its maximum adsorption capacity. As can be seen in Fig. 1, for Cd^{2+} adsorption, the end of the curve is almost transformed into a straight line. It implies that adsorption sites are practically saturated at higher concentrations.

2. Comparison of Copper and Cadmium Adsorption

The experimental data are well-fitting in with Langmuir, Freundlich, and Dubinin-Radushkevich models (Table 1). The Freundlich

Table 1. Constants and determination coefficient of Langmuir, Freundlich, and Dubinin-Radushkevich models fitting to adsorption results

Heavy metal	Langmuir			
	q_{max} (mg/g)	K_L	R^2	SEE
Cu^{2+}	21.24±1.09	0.132±0.033	0.93	2.18
Cd^{2+}	19.63±1.09	0.084±0.022	0.93	1.96
	Freundlich			
	n	$K_{F,ads}$	R^2	SEE
Cu^{2+}	0.214±0.007	7.33±0.22	0.99	0.61
Cd^{2+}	0.305±0.015	4.34±0.28	0.98	0.93
	Dubinin-Radushkevich			
	$q_{m,DR}$ (mol/g)	K_{DR} (mol^2/kJ^2)	E (kJ/mol)	R^2	SEe
Cu^{2+}	$5.3\times10^{-4}\pm2.1\times10^{-5}$	$2.1\times10^{-3}\pm1.2\times10^{-4}$	15.4	0.98	8.3×10^{-6}
Cd^{2+}	$3.75\times10^{-4}\pm2.03\times10^{-5}$	$2.87\times10^{-3}\pm1.5\times10^{-4}$	13.2	0.98	8.2×10^{-6}
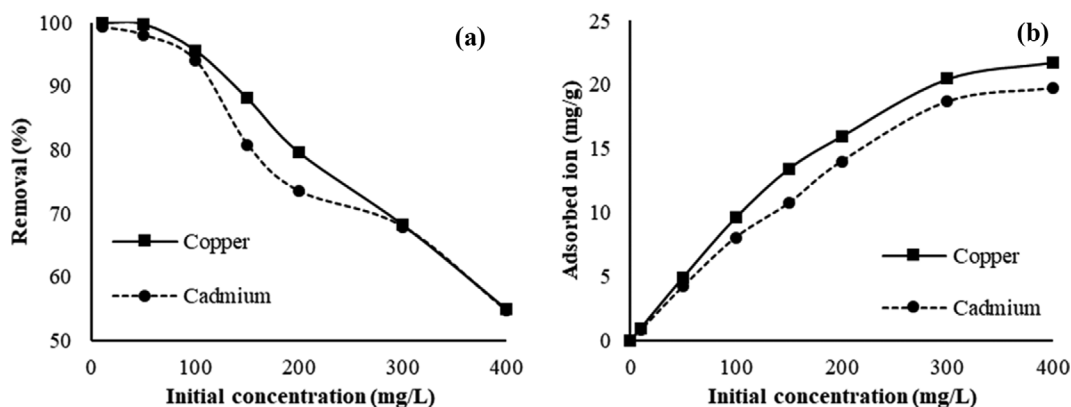
Fig. 2. (a) Removal efficiency of Cu^{2+} and Cd^{2+} in single mode, (b) Comparison of single adsorption of Cu^{2+} and Cd^{2+}.

and Dubinin-Radushkevich models have the highest R^2 coefficient and lowest SEE (standard error of estimate) in comparison to Langmuir, which indicates that the fitting of the Freundlich and Dubinin-Radushkevich models is better than the Langmuir for describing the adsorption of both studied heavy metals.

The maximum adsorption capacity (q_{max}) of the Langmuir model for Cu^{2+} and Cd^{2+} is 21.24 and 19.63 mg/g, respectively, which is higher than the experimental values. The difference could be because the theoretical model assumes the adsorption sites to form a single layer across the entire surface of the adsorbent [55]. The K_L is related to the adsorption tendency between adsorbate and adsorbent. This coefficient is higher for Cu^{2+} than Cd^{2+} indicating a higher tendency for Cu^{2+} uptake. The coefficient n in the Freundlich model is a measure of adsorption favorability and adsorbent surface heterogeneity, which is lower than 1 for Cu^{2+} and Cd^{2+}, implying that the adsorption of Cu^{2+} and Cd^{2+} by MNP is favorable and heterogeneous [56]. As presented in Table 1, the values of adsorption free energy (E) are higher than 8 (kJ/mol) for both ions. According to the literature, it can be deduced that the adsorption process pro-

ceeds by chemical adsorption, which occurs between adsorbent and metal ions [57].

Fig. 2(a) depicts the removal percentage of heavy metals by MNP. At 10 mg/L, 100% and 99.25% of Cu^{2+} and Cd^{2+} were removed, respectively. Subsequently, increasing the concentration of heavy metals in the solution caused a significant reduction in removal efficiency. Finally, MNP removed 54.8% and 54.6% of Cu^{2+} and Cd^{2+} at 400 mg/L, respectively. During the removal process, the majority of surface adsorption sites were covered by heavy metal ions. Therefore, the uptake performance was reduced in higher concentrations due to the lack of access to free active sites. As a result, owing to the abundance of active sites on the surface of the adsorbent, the removal efficiency improved at low concentrations [58].

So far, numerous studies have been conducted on the single adsorption of Cu^{2+} and Cd^{2+} by different materials. Note that the maximum adsorption capacity relies on various factors, including the quantity of adsorbent and adsorbate, specific surface area and porosity of adsorbent, contact time, and environmental conditions

Table 2. Comparison of the efficiency of MNP with that of previous studies

Adsorbent	Adsorption capacity (mg/g)		Reference
	Cu^{2+}	Cd^{2+}	
MNP	21.24	19.63	Current study
Few-layered magnetic graphene oxide	1,114.22	401.14	[59]
Coconut coir activated carbon	84.74	68.03	[60]
Ca-bentonite	7.72	7.28	[61]
Na-bentonite	30	26.2	
Gasifier Biochar	83.7	68.6	[62]
Nitrilotriacetic acid silica gel	63.51	53.14	[63]
Tourmaline	78.86	66.67	[64]
Magnetite/carbon nanocomposites	182.59	158.93	[65]
Magnetic DHPDT-Zeolite	181.82	178.57	[66]
Magnetic NaY Zeolite	107.53	108.7	
Sodium alginate composite gel	6.783	3.426	[67]
$CaCO_3$/chitin hydrogel	194.61	191.58	[68]
Ghassoul clay	15.41	86.34	[69]
Lignite	21.4	38	[70]

such as temperature and pH. Hence, a comparison of the maximum removal capacity of heavy metal ions by different adsorbents of different studies would be inequitable. Despite this, the comparison of the maximum single adsorption capacity of Cu^{2+} and Cd^{2+} with other relevant studies is reported in Table 2. MNP outperformed the adsorbents of some previous studies and showed less adsorption than some others, but the importance of this adsorbent is that it is environmentally friendly and is green-synthesized from industrial iron waste using green tea extract.

3. Adsorption Mechanisms

Different mechanisms, such as ion exchange, surface complexation, dissolution/precipitation, electrostatic interactions, structural incorporation, and oxidation/reduction can be considered for heavy metals adsorption [71,72]. As seen in Fig. 2(b), Cu^{2+} adsorption is higher than Cd^{2+}. This difference can be attributed to the difference in electrostatic interaction between heavy metal ions and adsorbent sites [73] and adsorption mechanisms. Many aspects, including ionic radius, chemical properties, hydrolysis constant, and ionic potential q/r (q is the ionic charge and r is the ionic radius) affect the adsorption of heavy metal ions [74]. The characteristics of Cu^{2+} and Cd^{2+} are presented in Table 3.

Hydrated ionic radius may influence the interaction of ions with negatively charged sites. The interspace to the adsorbent surface increases as the hydrated ionic radius increases. This phenomenon weakens the adsorption process [73]. The Cu^{2+} has a higher ionic potential (2.8), compared to Cd^{2+} (1.9) [74], and a smaller hydrated ionic radius (0.419 nm), in comparison with Cd^{2+} (0.426 nm) [75]. As a result, Cu^{2+} ions can gain greater access to surfaces

Table 3. Properties of Cu^{2+} and Cd^{2+} cations [82,83]

Property	Cu^{2+}	Cd^{2+}
Molecular weight (g/mol)	63.556	112.4
Ion radius (Å)	0.73	0.95
Atomic radius (Å)	1.57	1.71
Hydrated ion radius (Å)	4.19	4.26
Ionic potential	2.8	1.9
Standard reduction potential (V) $M^2+2e \rightarrow M(V)$	0.342	−0.403
Hydrolysis constant	8	10.1
Electronegativity (Pauling)	1.9	1.69

and pores, leading to penetration into smaller pores. It could be concluded that Cu^{2+} has a higher adsorption capacity than Cd^{2+}. Another reason for the higher adsorption of Cu^{2+} than Cd^{2+} could be due to the electronegativity difference between the two ions and, in this regard, Renugopal et al. [76] reported higher percentage removal of Cu^{2+} compared to Cd^{2+}. Also, standard reduction potential of ions can affect their adsorption affinity [77] and the heavy metals can be adsorbed via reduction/oxidation reactions. Due to the presence of the Fe^{2+} ion, MNP can serve as electron donors [78] and can reduce metals when the redox potential of heavy metals is higher than that of Fe_2O_3/Fe_3O_4 pair [79]. Cu^{2+} has a higher standard reduction potential (0.342 V) than Fe_2O_3/Fe_3O_4 (0.009 and 0.29 V) [80]. Therefore, the reduction of Cu^{2+} and conversion to Cu^0 can be considered as a possible mechanism for Cu^{2+}
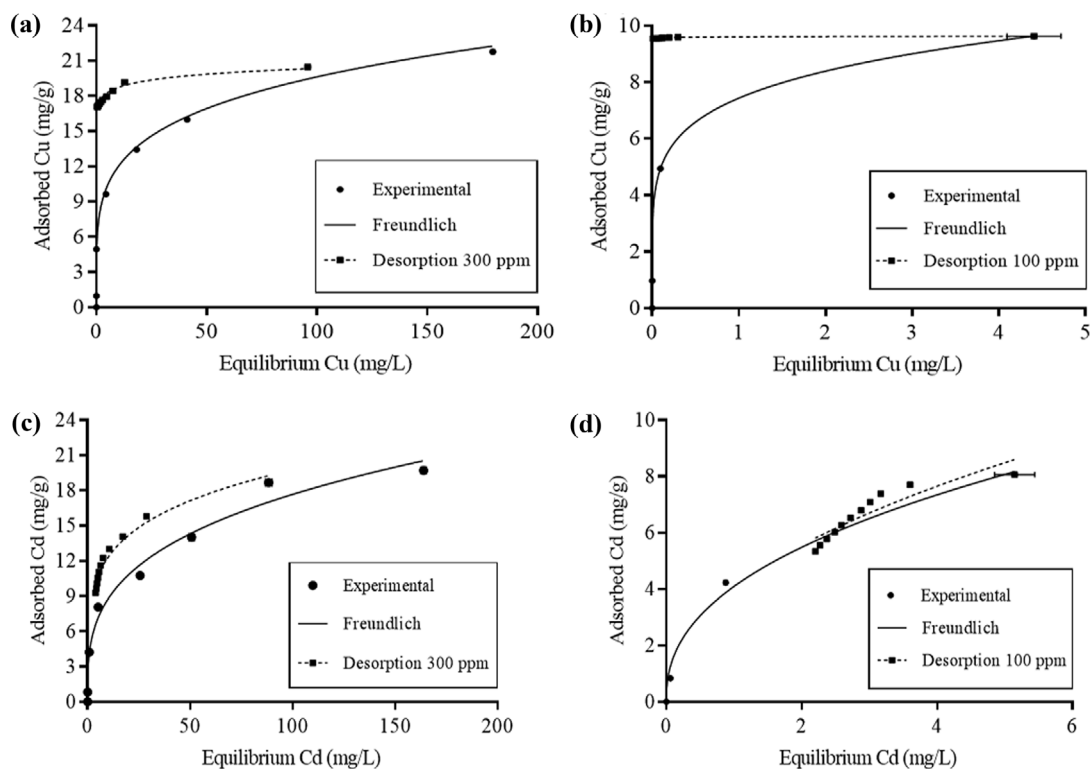

Fig. 3. Adsorption-desorption isotherm by MNP: (a) Cu^{2+} initial concentration of 300 mg/L, (b) Cu^{2+} initial concentration of 100 mg/L, (c) Cd^{2+} initial concentration of 300 mg/L, (d) Cd^{2+} initial concentration of 100 mg/L.

Table 4. Constants and determination coefficient of Freundlich model fitting to desorption results

Heavy metal	Initial concentration (mg/L)	n	$K_{F, des}$	R^2	SEE
Cu^{2+}	100	0.002±0.0003	9.604±0.006	0.888	0.011
	300	0.036±0.002	17.25±0.08	0.962	0.22
Cd^{2+}	100	0.463±0.066	4.029±0.304	0.835	0.385
	300	0.206±0.012	7.649±0.274	0.963	0.579

Table 5. Hysteresis indexes of Cu^{2+} and Cd^{2+} desorption

Heavy metal	Initial concentration (mg/L)	n_{des}	n_{ads}	H	ω	λ
Cu^{2+}	100	0.002	0.214	0.93	10,600	21.16
	300	0.036		16.82	494.4	17.18
Cd^{2+}	100	0.463	0.305	151.8	−34.13	−10.8
	300	0.206		67.54	48.06	8.2

adsorption [81]. However, because of the lower standard reduction of Cd^{2+} (−0.403 V), the reduction mechanism cannot play a role in Cd^{2+} removal and sorption is the main mechanism.

4. Single Desorption Studies

Fig. 3 shows Cu^{2+} and Cd^{2+} adsorption-desorption isothermal curves. According to Figs. 3(a) and 4(b), the Cu^{2+} released from MNP is negligible. This reflects the irreversible adsorption and strong bonding between adsorbent and adsorbate. In none of the concentrations of Cu^{2+}, the adsorption and desorption isotherms matched together, which indicates that MNP does not desorb the total amount of adsorbed Cu^{2+}. The sample with 100 mg/L initial concentration had a higher hysteresis than the sample with 300 mg/L primary concentration. It means that adsorption shifts from strong to weak adsorption as the initial concentration rises. The adsorption-desorption isothermal graphs of Cd^{2+} with two primary concentrations of 100 and 300 mg/L are shown in Fig. 3(c) and 3(d), respectively. As can be observed, MNP releases a significant amount of Cd^{2+}, which is due to the reversibility of adsorption and physical interaction between the adsorbent and adsorbate. The Cd^{2+} adsorption and desorption had more coincidence and lower hysteresis than Cu^{2+} at both concentrations. Moreover, the hysteresis of the 100 mg/L sample was lower than 300 mg/L. In the 100 mg/L samples, the amount of released Cd^{2+} in the desorption process was higher than the predicted amount of adsorption. Thus, in equilibrium conditions, for a certain concentration of Cd^{2+}, the amount of adsorbed Cd^{2+} from adsorption isotherm was lower than the values determined by its corresponding desorption, indicating negative hysteresis [84]. The desorption rate of the 300 mg/L samples decreased considerably over time, while the Cd^{2+} release rate of the 100 mg/L sample did not reduce by the end of the 10-day cycle and that can be related to negative hysteresis being responsible for this phenomenon.

Table 4 presents the constants and coefficients of the Freundlich model fitting to desorption experimental results. The n coefficient of both Cu^{2+} concentrations is much lower than the adsorption coefficient, indicating that MNP has a much stronger tendency to retain Cu^{2+} than to release it. $K_{F, des}$ showed a reversal trend, with the amount of this coefficient being lower in adsorption than desorp-

tion. In comparison to Cu^{2+} desorption, the n coefficient for Cd^{2+} desorption was greater, indicating a higher tendency to release it. The smaller K_F coefficient values, in contrast to the n coefficient, result in higher desorption. The R^2 and SEE coefficients indicated the proper fit of the Freundlich model with the desorption data.

Table 5 shows hysteresis indices, all of which are calculated according to the equations of Gao and Jiang [51] (section 2.4 in Materials and Methods). The MNP has positive hysteresis for both Cu^{2+} concentrations, as measured by the values of H, ω, and λ. According to Barriuso et al. [50], in the system of 100 mg/L of Cd^{2+}, $n_{des}/n_{ads} > 1$ and $K_{des} < K_{ads}$ indicate a negative hysteresis. Furthermore, the desorption isotherm graph demonstrates this phenomenon (Fig. 3(d)). Finally, a positive hysteresis was found for Cd^{2+} at 300 mg/L.

5. Comparison of Copper and Cadmium Desorption

Table 6 presents the average desorption percentage of heavy metals after ten cycles of dilution. The majority of the Cu^{2+} adsorbed by MNP remained on the adsorbent after ten days. Consequently, Cu^{2+} adsorption by MNP seems to be irreversible. A large portion of the adsorbed Cd^{2+} was desorbed after ten days. It could be concluded that Cd^{2+} adsorption on MNP is reversible and non-

Table 6. Cumulative desorption percentages of Cu^{2+} and Cd^{2+} in a 10-day cycle

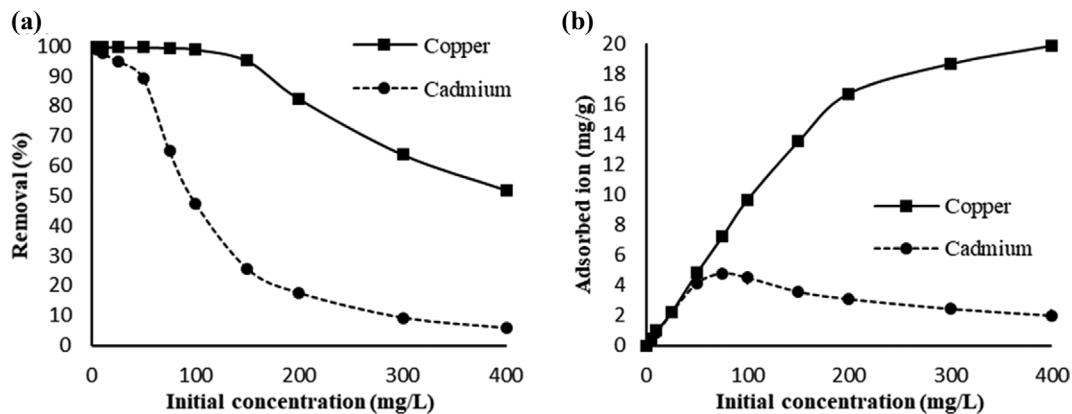| Initial conc. (mg/L) Days	Cu^{2+}		Cd^{2+}	
	100	300	100	300
1	0.31	6.29	4.47	15.38
2	0.51	9.97	8.4	24.59
3	0.64	12.26	12.13	30.29
4	0.75	13.64	15.7	34.36
5	0.84	14.63	19.08	37.77
6	0.89	15.31	22.28	40.8
7	0.9	15.79	25.37	43.52
8	0.9	16.17	28.31	46
9	0.9	16.43	31.13	48.28
10	0.9	16.66	33.86	50.38

Fig. 4. (a) Removal efficiency of Cu^{2+} and Cd^{2+} in competitive mode, (b) Comparison of competitive adsorption of Cu^{2+} and Cd^{2+}.

specific with cation exchange (outer-sphere complex) as the primary mechanism [84].

6. Competitive Adsorption Studies

Fig. 4(a) depicts the percentage of heavy metals removal under competitive conditions. For Cu^{2+} concentrations up to 100 mg/L, MNP had a removal rate of over 99%. However, the removal efficiency decreased at higher concentrations. The Cu^{2+} removal reached 51.8% at the highest concentration. The removal efficiency of Cd^{2+} declined dramatically as the initial concentration increased. The removal percentage was 98.9% at the lowest primary concentration, but it decreased to 5.8% at 400 mg/L. The MNP was able to sustain a high level of removal up to 50 mg/L followed by a decline.

Fig. 4(b) illustrates the adsorption amount of each heavy metal in competitive mode. Metal ions compete with each other for surface sites in a competitive system. As can be seen, the tendency of adsorbent for adsorbing Cu^{2+} is much greater than for Cd^{2+}. The amount of Cu^{2+} adsorption increased with the higher initial concentration of heavy metals in the solution. On the other hand, Cd^{2+} adsorption peaked at 75 mg/L, and then, as the primary concentration increased, the amount of Cd^{2+} adsorption decreased. As shown in Fig. 4(b), MNP adsorbs Cu^{2+} at a high rate up to 200 mg/L, after which the adsorption rate continues with a lower slope. The diminishing rate is probably related to the saturation of adsorption sites. The maximum adsorption of Cu^{2+} by MNP was 19.82 mg/g at 400 mg/L. The process of adsorption of Cd^{2+} by MNP up to 50 mg/L was similar to that of Cu^{2+} and then was defeated by Cu^{2+}. The maximum uptake of Cd^{2+} was observed at a concentration of 75 mg/L (4.78 mg/g) and then the trend decreased. Therefore, adsorption at 400 mg/L decreased to 1.9 mg/g (58.3% reduction, compared to the maximum adsorbed amount).

The distribution coefficient (K), which is a measure of the difficulty in adsorbing ions by an adsorbent, can be employed to determine the affinity of MNP with different ions. Higher values of K indicate the ease of adsorption of metal ions to the adsorbent. The lower the amount, the harder it is to adsorb ions [85]. Distribution coefficient is defined as Eq. (10).

$$K = \frac{q_e}{C_e} \qquad (10)$$

where q_e represents adsorption capacity at equilibrium (mg/g)

and C_e is the concentration of adsorbate at equilibrium (mg/L). For all studied concentrations in range of 5-400 mg/L, K values were always higher for Cu^{2+} than that of Cd^{2+}. For instance, at 400 mg/L, K was 0.108 and 0.006 L/g for Cu^{2+} and Cd^{2+}, respectively. This result indicates that MNP has a higher affinity with Cu^{2+} in comparison with Cd^{2+} in competitive media. It can be stated that MNP is selective for Cu^{2+}. Castañeda-Ramírez et al. [86] reported that magnetite nanoparticles@Fe-BTC composite had higher distribution coefficient for Cu^{2+} and Pb^{2+} than Hg^{2+} and As^{2+}, which indicates that the adsorbent is selective for adsorbing Cu^{2+} and Pb^{2+} ions.

Chen and Xie [9] developed Fe_3O_4-MnO_2 and Fe_3O_4-MnO_2-EDTA magnetic nanoparticles to investigate selective adsorption of Cu^{2+} with a variety of metal ions, including Cd^{2+} in binary and ternary systems. For both adsorbents, Cd^{2+} was less adsorbed in comparison to Cu^{2+} in a binary system. Sun et al. [4] investigated competitive removal of Cu^{2+} and Cd^{2+} from alkaline solutions using chitosan-tannin functional paper. They stated that in lower concentrations, the presence of both ions did not considerably influence the adsorption. However, with the increase of heavy metals' concentration (greater than or equal to 200 mg/L), Cu^{2+} competed with Cd^{2+} for binding sites and Cd^{2+} adsorption capacity decreased by 18-52.8%. Dou et al. [68] synthesized $CaCO_3$/chitin hydrogel to evaluate the adsorption of Cu^{2+} and Cd^{2+} in single and binary systems. Although the adsorbate showed a high adsorption capacity for both ions in the single system, it exhibited more tendency in Cu^{2+} uptake than Cd^{2+}. All mentioned studies confirm the selective adsorption of Cu^{2+} against Cd^{2+} and minor effect of Cd^{2+} on Cu^{2+} uptake in competitive mode.

Some metal cation features, such as ionic radius, atomic weight, hydration energy, electronegativity, hydrolysis constant, and softness parameter, can influence metal adsorption preference by different adsorbents [87-89]. The results reveal that the impact of the presence of Cu^{2+} ions on Cd^{2+} adsorption was more remarkable than the effect of Cd^{2+} ions on Cu^{2+} uptake. It means that the adsorbent has a much higher affinity for Cu^{2+} metal ions than for Cd^{2+}. The greater adsorption of Cu^{2+} than Cd^{2+} is justified by a comparison of the properties of Cu^{2+} and Cd^{2+} (Table 3), such as ionic radius (0.73 Cu^{2+}<0.95 Cd^{2+}), hydrated ionic radius (4.19 Cu^{2+}< 4.26 Cd^{2+}), electronegativity (1/90 Cu^{2+}>1.69 Cd^{2+}), standard reduc-
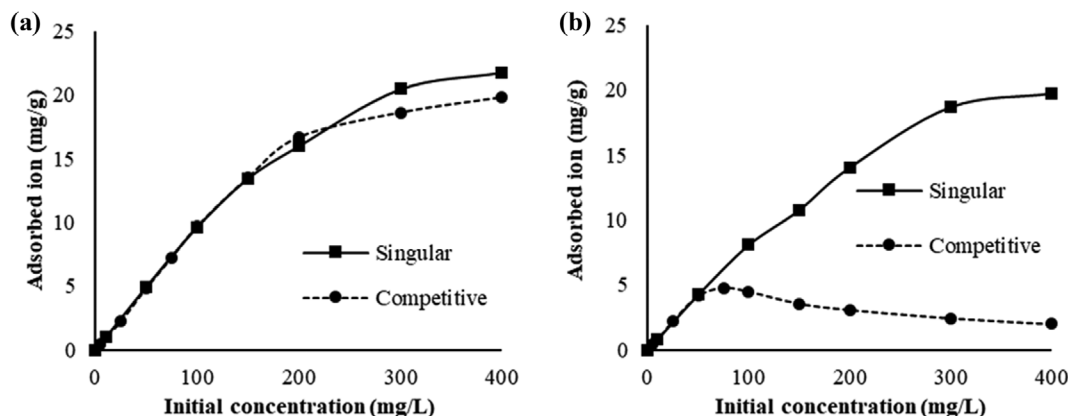
Fig. 5. Comparison of single and competitive adsorption (a) Cu^{2+}, (b) Cd^{2+}.

tion potential (0.342 V for Cu^{2+} and −0.403 for Cd^{2+}), as well as the constant difference in the hydrolysis of these two elements [89,90].

7. Comparison of Single and Competitive Adsorption

Fig. 5 compares the adsorption of Cu^{2+} and Cd^{2+} by single and competitive systems. Because of the high adsorption of Cu^{2+} in both systems and the defeat of Cd^{2+} in the competitive system (despite its permissible adsorption in single mode), comparing the two systems will help in understanding this phenomenon. In both systems, Cu^{2+} adsorption follows a similar pattern. As a result, both diagrams are almost equal to up to 150 mg/L. At 200 mg/L, the amount of Cu^{2+} adsorption in the competitive state is slightly higher than the single state, and at 300 and 400 mg/L, this trend is reversed.

The single and competitive adsorptions of Cd^{2+} are very distinct from those of Cu^{2+}. For both conditions, trends are very similar at low concentrations But at concentration over 75 mg/L, the adsorption process differs significantly. The amount of adsorption increases as the initial concentration rises in the single mode. However, in competitive mode, the higher the primary concentration, the lower the Cd^{2+} adsorption. The diagrams show that the adsorbent removed Cu^{2+} properly, regardless of the presence or absence of Cd^{2+} in the solution and that the operation was not disrupted at the presence of Cd^{2+}. In competitive mode, a higher proportion of Cu^{2+} was removed at the concentrations of 75-200 mg/L, which may be attributed to experimental conditions. Although Cd^{2+} had been well removed from the aqueous solution in single mode, the adsorbent preferred Cu^{2+} in the competitive state. In the single system, the similarities between the removal efficiency of Cu^{2+} and Cd^{2+} increased as the initial concentration of metal ions increased. Despite such circumstances, it was extremely difficult to predict the results of the competitive system.

8. Competitive Desorption Studies

Over a ten-day cycle, competitive desorption of Cu^{2+} and Cd^{2+} was examined for samples with the initial concentrations of 50 and 150 mg/L. Fig. 6(a) shows the competitive desorption daily. As demonstrated in Fig. 6, Cu^{2+} desorption is negligible, compared to its adsorption, and decreases over time. On the other hand, the amount of desorption in the 150 mg/L samples decreases more than 50 mg/L over time. This is probably attributed to higher concentrations of Cu^{2+} penetrating through the adsorbent pores. The Cd^{2+} desorption results presented in Fig. 6(a) for both 150 and
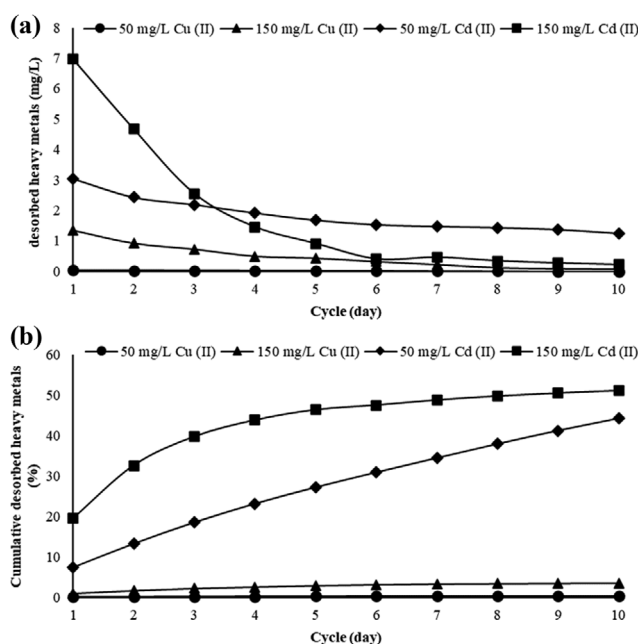

Fig. 6. Competitive desorption of Cu^{2+} and Cd^{2+}, (a) The amount of desorption per day, (b) The cumulative percentage of desorption.

50 mg/L samples indicate that Cd^{2+} desorption is much higher than Cu^{2+}. This is in agreement with the findings of single desorption analyses. Same as Cu^{2+}, Cd^{2+} desorption for the sample with higher concentration declined more significantly over time. In contrast to the first day, the amount of Cd^{2+} desorption for the 150 mg/L samples decreased by more than 32 times on the tenth day. In contrast, the amount of desorption on the tenth day was still significant in the sample of 50 mg/L.

The Cd^{2+} was desorbed at a higher rate per day from a 150 mg/L sample. While Cd^{2+} adsorption was much lower than Cu^{2+} in the competitive state, it was desorbed at a higher rate. This might be attributed to the physical adsorption of Cd^{2+} on the adsorbent and its lower penetration into pores, compared to Cu^{2+} due to the larger hydrated radius. However, a considerable amount of Cd^{2+} was released from the adsorbent during the desorption period. More
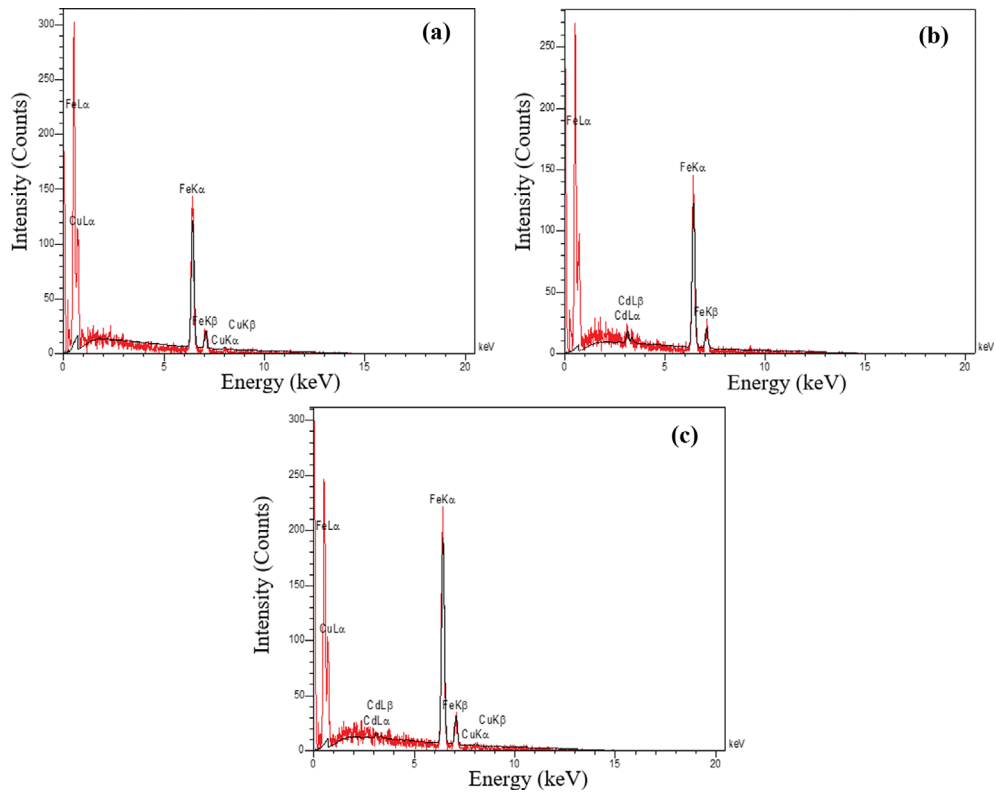
Fig. 7. EDX spectrum after adsorption (a) Singular Cu^{2+}, (b) Singular Cd^{2+}, (c) Competitive mode.
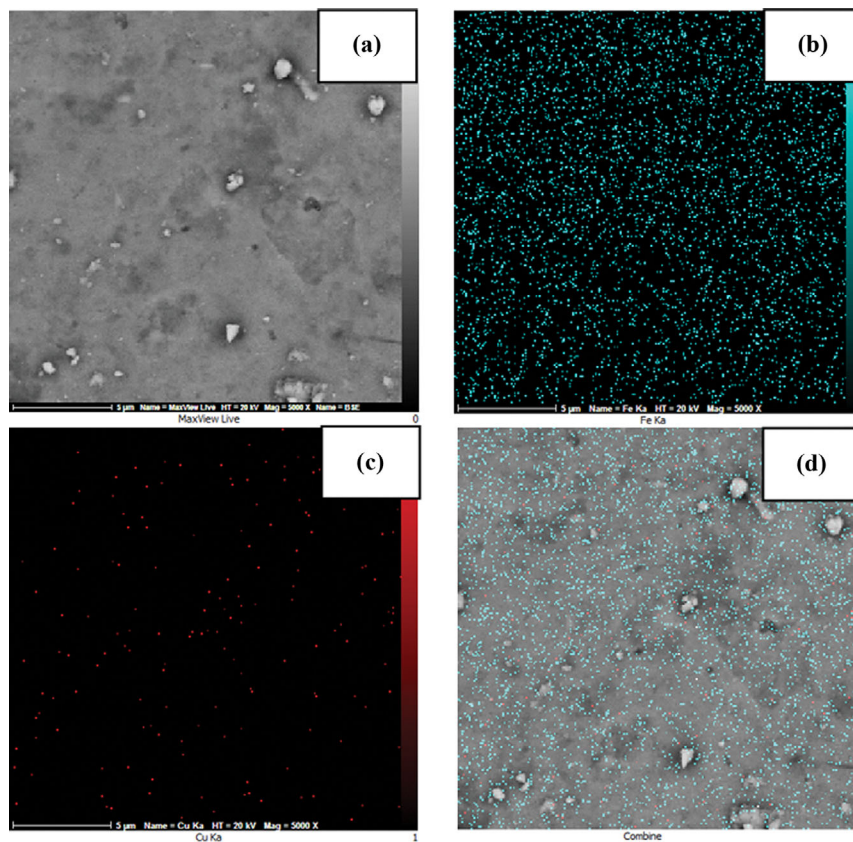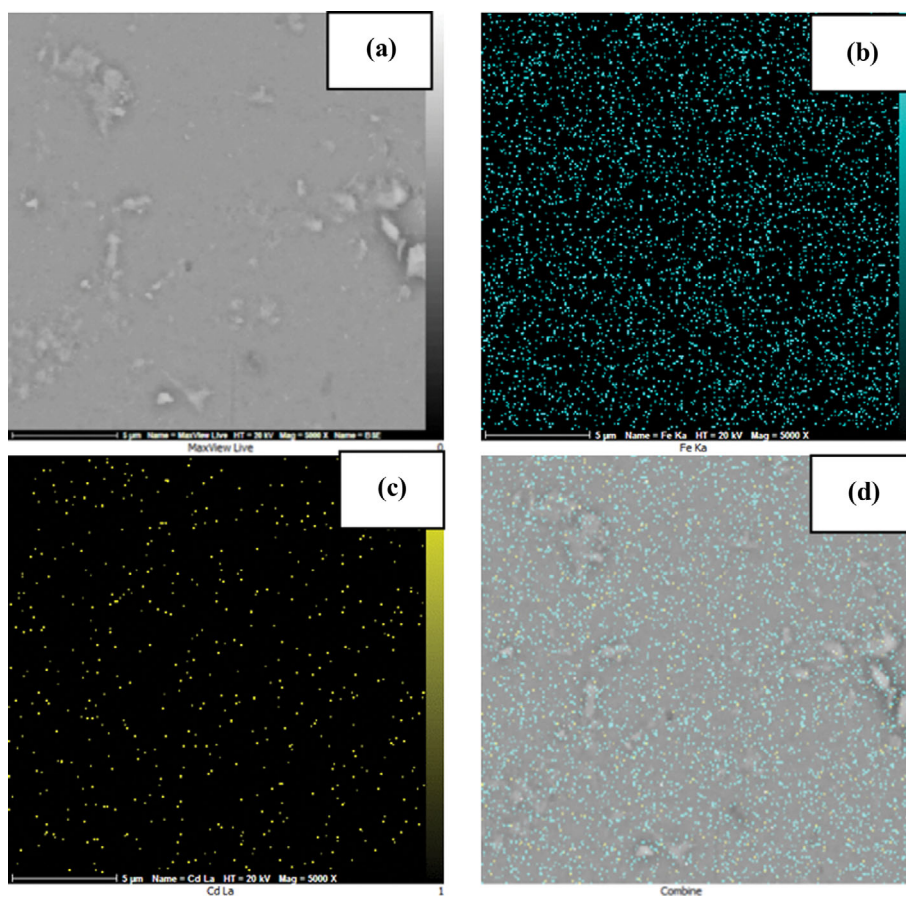

Fig. 8. Results of Elemental Mapping after Cu^{2+} adsorption, (a) sample surface, (b) Fe elements, (c) adsorbed Cu^{2+} on the adsorbent surface, (d) composition of images.

Fig. 9. Results of Elemental Mapping after Cd^{2+} adsorption, (a) sample surface, (b) Fe elements, (c) adsorbed Cd^{2+} on the adsorbent surface, (d) composition of images.

than 40% and 50% of the adsorbed Cd^{2+} was released from the samples of 50 and 150 mg/L, respectively.

9. Characterization of the Spent Adsorbent

Following the completion of adsorption tests in single and competitive modes, EDX, elemental mapping, and FTIR analyses were performed on the samples with the highest initial concentrations of Cu^{2+} and Cd^{2+}.

9-1. Energy-dispersive X-ray (EDX)

Fig. 7(a)-(c) illustrates the EDX spectrum after adsorption. Peaks in the Cu^{2+} adsorption range (8A) with energy levels of around 0.5, 6.4, and 7.1 keV correspond to the X-ray emission of Lα, Kα, and Kβ of iron, respectively. Moreover, peaks of 0.7, 8.1, and 8.8 keV are related to the emission beams of Lα, Kα, and Kβ of Cu^{2+}, respectively. According to the Cd^{2+} uptake spectrum in Fig. 7(b), in addition to the Lα, Kα, and Kβ of iron peaks discussed earlier, the Lα and Lβ peaks of Cd^{2+} are observed at the energy values of 3.1 and 3.3 keV. The Cd^{2+} and Cu^{2+} peaks are less intense than iron peaks. All the iron, Cu^{2+}, and Cd^{2+} peaks studied in the previous figures are observed in the competitive adsorption of Cu^{2+} and Cd^{2+} confirming the competitive adsorption of these two elements. As shown in Fig. 7(c), Cu^{2+} has a higher peak intensity than Cd^{2+}.

9-2. Elemental Mapping

Figs. 8-10 represent the distribution of Cu^{2+} and Cd^{2+} ions on the MNP surface after the completion of the single and competi-

tive states. As shown, the adsorbent could uptake Cu^{2+} (red) and Cd^{2+} (yellow). It is noteworthy that Cd^{2+} is more abundant than Cu^{2+} (despite higher Cu^{2+} adsorption) in all figures. The exterior surface of the samples was subjected to element mapping analysis [91,92]. The higher Cd^{2+} abundance means that more Cd^{2+} ions are likely to be physically adsorbed on the outer surface of the adsorbents. However, Cu^{2+} is chemically adsorbed with stronger bonds in the porous structure of the adsorbents. This is consistent with the results of the single and competitive desorption experiments.

9-3. Fourier-transform Infrared Spectroscopy (FTIR)

Fig. 11 depicts the infrared spectrum before and after adsorption. The Fe-O group and the magnetite structure are represented by bands 439, 540, and 640 cm^{-1} in the MNP (Fig. 11(a)). The bands 439 and 640 cm^{-1} have shifted during Cd^{2+} uptake (Fig. 11(b), while the band 540 cm^{-1} has remained unchanged. However, in Cu^{2+} adsorption (Fig. 11(c)), the band 540 cm^{-1} has been displaced, while the bands 439 and 640 cm^{-1} have not changed. In the competitive state, though, all three Fe-O bands were involved in the adsorption process and were displaced (Fig. 11(d)). A parallel pattern was observed in the 825 and 1,064 cm^{-1} bands, with the first band being displaced only in Cd^{2+} removal and the second one being displaced in both individual Cu^{2+} and competitive adsorption. Consequently, in both single and competitive states, the carboxylate functional
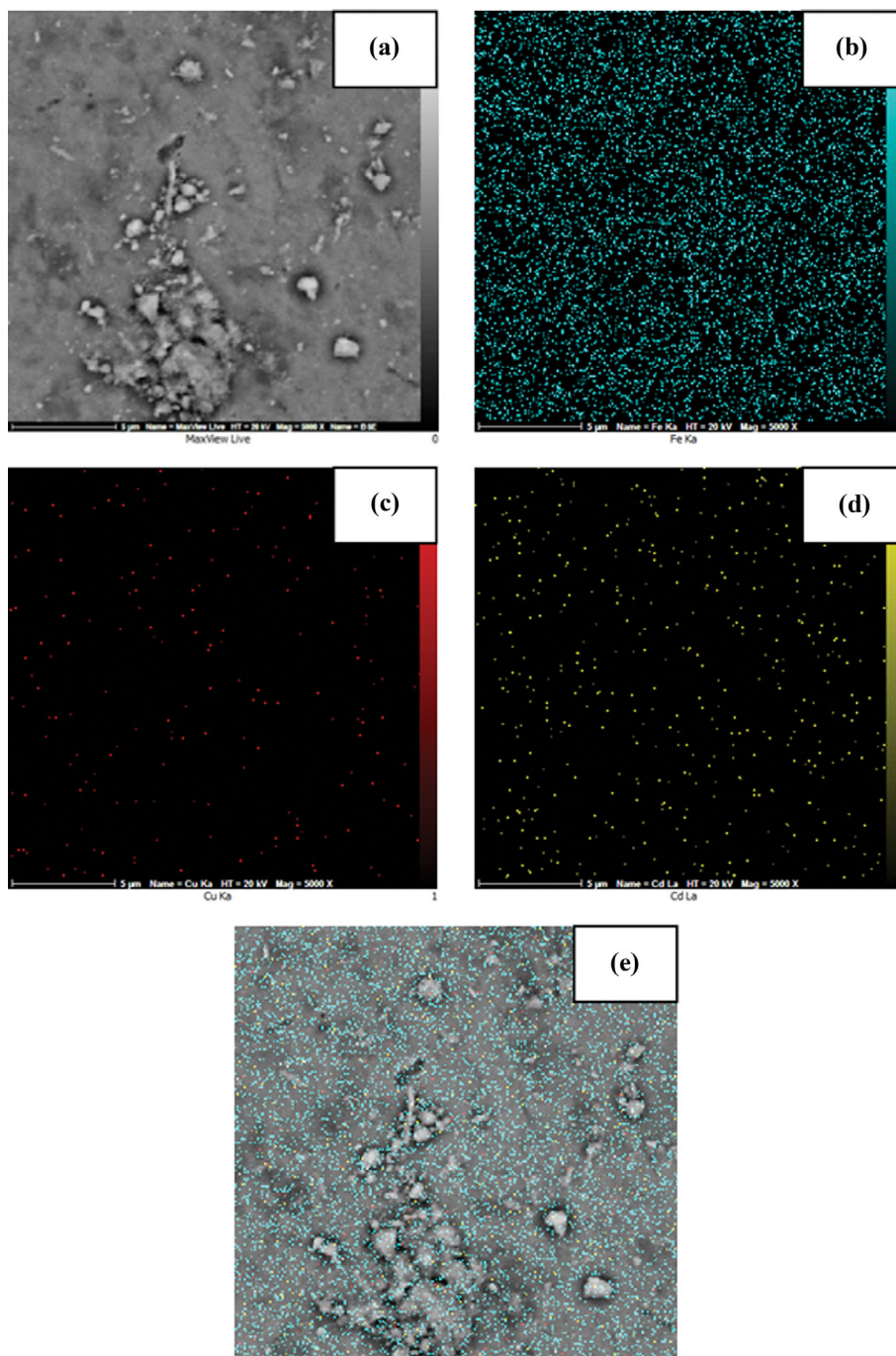
Fig. 10. Results of Elemental Mapping after competitive adsorption, (a) sample surface, (b) Fe elements, (c) adsorbed Cu^{2+} on the adsorbent surface, (d) adsorbed Cd^{2+} on the adsorbent surface, (e) composition of images.

group (COO-) may have been involved in Cu^{2+} uptake. Jin et al. [93] confirmed Cu^{2+} ion adsorption through weak interactions between metal and carboxylate. In comparison to the 825 cm^{-1} band, the 1,627 cm^{-1} band has been displaced through Cd^{2+} uptake. Both bands assumed to be related to aromatic compounds played a role in Cd^{2+} removal. Harvey et al. [94] in research focused on the role of aromatic groups in Cd^{2+} ion uptake. Kataria and Garg [95] examined the role of the carbonyl functional group in Cd^{2+} uptake. Overall, the findings revealed that functional groups were actively involved

in the adsorption of Cu^{2+} and Cd^{2+} in both single and competitive states and formed chemical bonds with metal ions.

CONCLUSION

The adsorption capacity of green synthesized MNP was investigated for Cu^{2+} and Cd^{2+} in two single and competitive modes. The results demonstrated a strong adsorption tendency for both Cu^{2+} and Cd^{2+} in the single system, with more than 50% of contami-
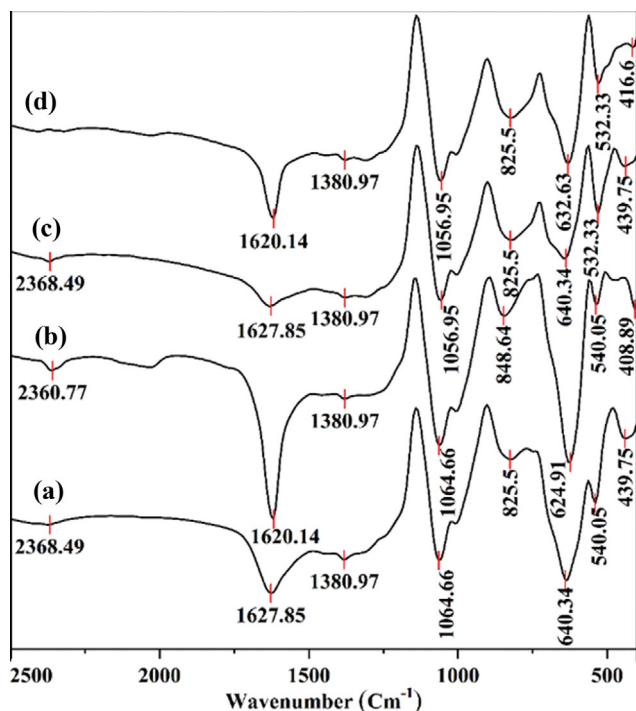
Fig. 11. FTIR spectroscopy of (a) before adsorption,(b) after single adsorption of Cd^{2+}, (c) after single adsorption of Cu^{2+}, (d) after competitive adsorption.

nants eliminated at a primary concentration of 400 mg/L. However, in the binary system, the adsorbent favored Cu^{2+} over Cd^{2+}. As the initial concentration of metal ions in the competitive condition increased, Cu^{2+} adsorption constantly increased. On the other hand, Cd^{2+} adsorption decreased after 75 mg/L. The removal efficiency of Cu^{2+} and Cd^{2+} in the highest studied concentrations of the competitive method was 51.8% and 5.8%, respectively. The findings of desorption experiments in both single and competitive systems reveal that the adsorbent selectively retained Cu^{2+} over Cd^{2+}. Overall, the use of synthesized adsorbent in the adsorptive removal of Cu^{2+}, in comparison with Cd^{2+} can be recommended due to the sufficient adsorption capacity of MNP in both individual and competitive systems.

ACKNOWLEDGEMENTS

REFERENCES

1. W. S. Chai, J. Y. Cheun, P. S. Kumar, M. Mubashir, Z. Majeed, F. Banat, S.-H. Ho and P. L. Show, *J. Cleaner Production*, **296**, 126589 (2021).
2. C. Zamora-Ledezma, D. Negrete-Bolagay, F. Figueroa, E. Zamora-Ledezma, M. Ni, F. Alexis and V. H. Guerrero, *Environ. Technol. Innovation*, **22**, 101504 (2021).
3. B. J. Ni, Q. S. Huang, C. Wang, T. Y. Ni, J. Sun and W. Wei, *Chemosphere*, **219**, 351 (2019).
4. H. Sun, N. Xia, Z. Liu, F. Kong and S. Wang, *Chemosphere*, **236**, 124370 (2019).
5. N. Arancibia-Miranda, K. Manquián-Cerda, C. Pizarro, T. Maldonado, J. Suazo-Hernández, M. Escudey, N. Bolan and B. Sarkar, *J. Hazard. Mater.*, **398**, 122940 (2020).
6. Z. Liu, X. Li, P. Zhan, F. Hu and X. Ye, *Sep. Purif. Technol.*, **206**, 199 (2018).
7. M. Khodakarami and M. Bagheri, *J. Clean. Prod.*, **296**, 126404 (2021).
8. A. Yusuf, A. Al Jitan, C. Garlisi and G. Palmisano, *Chemosphere*, **278**, 130440 (2021).
9. S. Chen and F. Xie, *Appl. Surf. Sci.*, **507**, 145090 (2020).
10. F. Renault, B. Sancey, P. M. Badot and G. Crini, *Eur. Polym. J.*, **45**, 1337 (2009).
11. P. Li, Y.-X. Li, Y.-Z. Wu, Z.-L. Xu, H.-Z. Zhang, P. Gao and S.-J. Xu, *Environ. Res.*, **197**, 111040 (2021).
12. R. Goswami, A. Mishra, N. Bhatt, A. Mishra and P. Naithani, *Mater. Today: Proc.*, **46**, 10954 (2021).
13. R. Shahrokhi-Shahraki, C. Benally, M. G. El-Din and J. Park, *Chemosphere*, **264**, 128455 (2021).
14. X. Zhang, X. Wang, H. Qiu, X. Sun, M. Han and Y. Guo, *Colloids Surf. B: Biointerfaces*, **189**, 110876 (2020).
15. X. Yang, L. Liu, W. Tan, C. Liu, Z. Dang and G. Qiu, *Environ. Pollut.*, **264**, 114745 (2020).
16. T.-K. Tran, K.-F. Chiu, C.-Y. Lin and H.-J. Leu, *Int. J. Hydrogen Energy*, **42**, 27741 (2017).
17. K. Koczka and P. Mizsey, *Period. Polytech. Chem. Eng.*, **54**, 41 (2010).
18. G. Doornbusch, M. van der Wal, M. Tedesco, J. Post, K. Nijmeijer and Z. Borneman, *Desalination*, **505**, 114973 (2021).
19. K. H. Choi and T. Y. Jeoung, *Korean J. Chem. Eng.*, **19**, 107 (2002).
20. S. M. Hosseini, H. Alibakhshi, E. Jashni, F. Parvizian, J. N. Shen, M. Taheri, M. Ebrahimi and N. Rafiei, *J. Hazard. Mater.*, **381**, 120884 (2020).
21. A. Dąbrowski, Z. Hubicki, P. Podkościelny and E. Robens, *Chemosphere*, **56**, 91 (2004).
22. S. Satyro, M. Race, F. Di Natale, A. Erto, M. Guida and R. Marotta, *Chem. Eng. J.*, **283**, 1484 (2016).
23. R. Sharma, T. Jasrotia, R. Kumar, R. Kumar, A. A. Alothman, M. m. Al-Anazy, K. N. Alqahtani and A. Umar, *Chemosphere*, **276**, 130018 (2021).
24. M. Priyadarshanee and S. Das, *J. Environ. Chem. Eng.*, **9**, 104686 (2021).
25. Q. Kong, X. Shi, W. Ma, F. Zhang, T. Yu, F. Zhao, D. Zhao and C. Wei, *J. Hazard. Mater.*, **415**, 125690 (2021).
26. C. F. Carolin, P. S. Kumar, A. Saravanan, G. J. Joshiba and M. Naushad, *J. Environ. Chem. Eng.*, **5**, 2782 (2017).
27. F. Afroosheh, S. Bakhtiari, M. Shahrashoub and M. Ebrahimi, *J. Nano Res.*, **66**, 129 (2021).
28. M. I. Inyang, B. Gao, Y. Yao, Y. Xue, A. Zimmerman, A. Mosa, P. Pullammanappallil, Y. S. Ok and X. Cao, *Crit. Rev. Environ. Sci. Technol.*, **46**, 406 (2016).
29. E. Vunain, A. K. Mishra and B. B. Mamba, *Int. J. Biol. Macromol.*, **86**, 570 (2016).
30. M. Marcos-Hernández, R. A. Arrieta, K. Ventura, J. Hernández, C. D. Powell, A. J. Atkinson, J. S. Markovski, J. Gardea-Torresdey,

K. D. Hristovski, P. Westerhoff, M. S. Wong and D. Villagrán, *Environ. Adv.*, **4**, 100046 (2021).

31. J.-H. Park, Y. S. Ok, S.-H. Kim, J.-S. Cho, J.-S. Heo, R. D. Delaune and D.-C. Seo, *Chemosphere*, **142**, 77 (2016).

32. M. Shahrashoub and S. Bakhtiari, *Micropor. Mesopor. Mater.*, **311**, 110692 (2021).

33. L. Giraldo, A. Erto and J. C. Moreno-Piraján, *Adsorption*, **19**, 465 (2013).

34. M. R. Lasheen, I. Y. El-Sherif, D. Y. Sabry, S. T. El-Wakeel and M. F. El-Shahat, *Desalin. Water Treat.*, **57**, 17421 (2016).

35. E. Darezereshki, A. k. Darban, M. Abdollahy and A. Jamshidi-Zanjani, *Environ. Nanotechnol., Monit Manage.*, **10**, 51 (2018).

36. L. P. Lingamdinne, Y.-Y. Chang, J.-K. Yang, J. Singh, E.-H. Choi, M. Shiratani, J. R. Koduru and P. Attri, *Chem. Eng. J.*, **307**, 74 (2017).

37. S. Bhattacharjee, F. Habib, N. Darwish and A. Shanableh, *Powder Technol.*, **380**, 219 (2021).

38. F. Almomani, R. Bhosale, M. Khraisheh, A. kumar and T. Almomani, *Appl. Surf. Sci.*, **506**, 144924 (2020).

39. U. A. Usman, I. Yusoff, M. Raoov and J. Hodgkinson, *Environ. Earth Sci.*, **78**, 615 (2019).

40. M. Shahrashoub, S. Bakhtiari, F. Afroosheh and M. S. Googheri, *Colloids Surf. A: Physicochem. Eng. Asp.*, **622**, 126675 (2021).

41. F. P. Fato, D.-W. Li, L.-J. Zhao, K. Qiu and Y.-T. Long, *ACS Omega*, **4**, 7543 (2019).

42. J. Yang, B. Hou, J. Wang, B. Tian, J. Bi, N. Wang, X. Li and X. Huang, *Nanomaterials* (Basel), **9**, 424 (2019).

43. M. R. Miri, R. Khosravi, A. A. Taghizadeh, M. Fazlzadehdavil, Z. Samadi, H. Eslami, A. Gholami and E. Ghahramani, *Desalin. Water Treat.*, **148**, 312 (2019).

44. M. Matouq, N. Jildeh, M. Qtaishat, M. Hindiyeh and M. Q. Al Syouf, *J. Environ. Chem. Eng.*, **3**, 775 (2015).

45. I. Langmuir, *J. Am. Chem. Soc.*, **40**, 1361 (1918).

46. H. Freundlich, *J. Phys. Chem.*, **57**, 1100 (1906).

47. M. M. Dubinin and L. V. Radushkevich, The equation of the characteristic curve of activated charcoal, *Proceedings of the Academy of Sciences*, 331 (1947).

48. X. Zhou, *J. Hazard. Mater.*, **384**, 121101 (2020).

49. M. Tanzifi, M. T. Yaraki, A. D. Kiadehi, S. H. Hosseini, M. Olazar, A. K. Bharti, S. Agarwal, V. K. Gupta and A. Kazemi, *J. Colloid Interface Sci.*, **510**, 246 (2018).

50. E. Barriuso, D. A. Laird, W. C. Koskinen and R. H. Dowdy, *Soil Sci. Soc. Am. J.*, **58**, 1632 (1994).

51. H.-J. Gao and X. Jiang, *Pedosphere*, **20**, 104 (2010).

52. K. Kavosi Rakati, M. Mirzaei, S. Maghsoodi and A. Shahbazi, *Int. J. Biol. Macromol.*, **130**, 1025 (2019).

53. M. Abbas, S. Kaddour and M. Trari, *J. Ind. Eng. Chem.*, **20**, 745 (2014).

54. C. H. Giles, T. H. MacEwan, S. N. Nakhwa and D. Smith, *J. Chem. Soc.*, 3973 (1960).

55. L. Molina, J. Gaete, I. Alfaro, V. Ide, F. Valenzuela, J. Parada and C. Basualto, *J. Mol. Liq.*, **275**, 178 (2019).

56. S. Fan, J. Chen, C. Fan, G. Chen, S. Liu, H. Zhou, R. Liu, Y. Zhang, H. Hu, Z. Huang, Y. Qin and J. Liang, *J. Hazard. Mater.*, **416**, 126225 (2021).

57. D. Balarak, F. Kord Mostafapour, H. Azarpira and A. Joghataei, Past name: *British J. of Pharmaceutical Research*, Past ISSN: 2231-2919,

58. X. Ma, L. Li, L. Yang, C. Su, K. Wang, S. Yuan and J. Zhou, *J. Hazard. Mater.*, **209-210**, 467 (2012).

59. T. Guo, C. Bulin, Z. Ma, B. Li, Y. Zhang, B. Zhang, R. Xing and X. Ge, *ACS Omega*, **6**, 16535 (2021).

60. M. Chaudhuri, S. R. M. Kutty and S. H. Yusop, *Nat. Environ. Pollut. Technol.*, **9**, 25 (2010).

61. E. Álvarez-Ayuso and A. García-Sánchez, *Clays Clay Miner.*, **51**, 475 (2003).

62. G. A. Burk, A. Herath, G. B. Crisler, D. Bridges, S. Patel, C. U. Pittman and T. Mlsna, *Front. Environ. Sci.*, **8**, 541203 (2020).

63. Y. Li, J. He, K. Zhang, T. Liu, Y. Hu, X. Chen, C. Wang, X. Huang, L. Kong and J. Liu, *RSC Adv.*, **9**, 397 (2019).

64. K. Jiang, T.-h. Sun, L.-n. Sun and H.-b. Li, *J. Environ. Sci.*, **18**, 1221 (2006).

65. A. Andelescu, M. A. Nistor, S. G. Muntean and M. E. Rădulescu-Grad, *Sep. Sci. Technol.*, **53**, 2352 (2018).

66. M. Shirani, A. Akbari and M. Hassani, *Anal. Methods*, **7**, 6012 (2015).

67. Y. Zhao, L. Zhan, Z. Xue, K. K. Yusef, H. Hu and M. Wu, *J. Chem.*, **2020**, 5496712 (2020).

68. D. Dou, D. Wei, X. Guan, Z. Liang, L. Lan, X. Lan, P. Liu, H. Mo and P. Lan, *J. Hazard. Mater.*, **423**, 127137 (2022).

69. K. El Ass, *Glob. Nest J.*, **20**, 198 (2018).

70. S. Jellali, A. A. Azzaz, M. Jeguirim, H. Hamdi and A. Mlayah, *Water*, **13**, 164 (2021).

71. M. Shi, X. Min, Y. Ke, Z. Lin, Z. Yang, S. Wang, N. Peng, X. Yan, S. Luo, J. Wu and Y. Wei, *Sci. Total Environ.*, **752**, 141930 (2021).

72. V. Kromah and G. Zhang, *Water*, **13**, 1843 (2021).

73. J. Yang, B. Hou, J. Wang, B. Tian, J. Bi, N. Wang, X. Li and X. Huang, *Nanomaterials*, **9**, 424 (2019).

74. B. Benguella and H. Benaissa, *Colloids Surf. A: Physicochem. Eng. Asp.*, **201**, 143 (2002).

75. E. R. Nightingale, *J. Phys. Chem.*, **63**, 1381 (1959).

76. L. Renugopal, K. W. Kow, P. L. Kiew, S. P. Yeap, H. S. Chua, C. H. Chan and R. Yusoff, *AIP Conference Proceedings*, **2124**, 020001 (2019).

77. W. Peng, H. Li, Y. Liu and S. Song, *J. Mol. Liq.*, **230**, 496 (2017).

78. L. Castro, M. L. Blázquez, F. González, J. A. Muñoz and A. Ballester, *Hydrometallurgy*, **179**, 44 (2018).

79. M. Bae, H. Lee, K. Yoo and S. Kim, *Hydrometallurgy*, **201**, 105560 (2021).

80. M. J. Bradley and P. G. Tratnyek, *ACS Earth Space Chem.*, **3**, 688 (2019).

81. D. Karabelli, Ç. Üzüm, T. Shahwan, A. E. Eroğlu, T. B. Scott, K. R. Hallam and I. Lieberwirth, *Ind. Eng. Chem. Res.*, **47**, 4758 (2008).

82. K. H. Gayer, *J. Chem. Ed.*, **54**, A429 (1977).

83. T. Bohli, A. Ouederni, N. Fiol and I. Villaescusa, *Comptes Rendus Chim.*, **18**, 88 (2015).

84. M. Hamidpour, M. Kalbasi, M. Afyuni, H. Shariatmadari, P. E. Holm and H. C. B. Hansen, *J. Hazard. Mater.*, **181**, 686 (2010).

85. B. Zeng, W. Wang, S. He, G. Lin, W. Du, J. Chang and Z. Ding, *Nano Mater. Sci.*, **3**, 429 (2021).

86. A. A. Castañeda-Ramírez, E. Rojas-García, R. López-Medina, D. C. García-Martínez, J. Nicolás-Antúnez and A. M. Maubert-Franco, *Catal. Today*, In press (2021).

1 (2017).

87. M. Zhang, Q. Yin, X. Ji, F. Wang, X. Gao and M. Zhao, *Sci. Rep.*, **10**, 3285 (2020).

88. J. Hur, J. Shin, J. Yoo and Y. S. Seo, *Sci. World J.*, **2015**, 836287 (2015).

89. K. He, Y. Chen, Z. Tang and Y. Hu, *Environ. Sci. Pollut. Res. Int.*, **23**, 2778 (2016).

90. R. Laus and V. T. de Fávere, *Bioresour. Technol.*, **102**, 8769 (2011).

91. S. Rajput, C. U. Pittman and D. Mohan, *J. Colloid Interface Sci.*, **468**, 334 (2016).

92. L. B. Tahar, M. H. Oueslati and M. J. A. Abualreish, *J. Colloid Interface Sci.*, **512**, 115 (2018).

93. S. Jin, B. C. Park, W. S. Ham, L. Pan and Y. K. Kim, *Colloids Surf. A: Physicochem. Eng. Asp.*, **531**, 133 (2017).

94. O. R. Harvey, B. E. Herbert, R. D. Rhue and L.-J. Kuo, *Environ. Sci. Technol.*, **45**, 5550 (2011).

95. N. Kataria and V. K. Garg, *Chemosphere*, **208**, 818 (2018).